Check for updates

Exfoliated graphite with spinel oxide as an effective hybrid electrocatalyst for water splitting†

Malgorzata Skorupska,[a] Kinga Kowalska,[a] Magdalena Tyc,[a] Anna Ilnicka, [ID] *[a] Mariusz Szkoda [ID] [bc] and Jerzy P. Lukaszewicz[ad]

The aim of the conducted research was to develop hybrid nanostructures formed from $MnCo_2O_4$ and exfoliated graphite. Carbon added during the synthesis allowed for obtaining a well-distributed $MnCo_2O_4$ particle size with exposed active sites contributing to the increased electric conductivity. The influence of the weight ratios of carbon to a catalyst for hydrogen and oxygen evolution reactions was investigated. The new bifunctional catalysts for water splitting were tested in an alkaline medium with excellent electrochemical performance and very good working stability. The results for hybrid samples show better electrochemical performance compared to the pure $MnCo_2O_4$. The highest electrocatalytic activity was for sample $MnCo_2O_4/EG$ (2/1), where the value of the overpotential was 1.66 V at 10 mA cm^{-2}, and also for this sample a low value of Tafel slope (63 mV dec^{-1}) was denoted.

In recent years, interest in carbon-based electrocatalysts has increased significantly, which has to do with their unique chemical properties and physical properties which are advantageous for the design of high-performance catalysts.[1–3] The development of carbon-based catalysts can not only reduce the use of precious metals but also create materials with high surface area, easy functionalization, and chemical stability.[1,4] In carbon–metal hybrid materials, transition metals exhibit remarkable catalytic abilities, while the carbon material provides better conductivity, greater surface area, prevents aggregation effects, and provides good dispersion of active centers.[2,5] In addition, interactions between carbon and metallic materials can change the properties of the whole hybrid, contributing to the formation of new active sites with enhanced adsorption capacity.[3,6] Consequently, many attempts have been made to develop such hybrids as potential candidates for electrochemical applications.[7] Hybrids based on carbon materials with transition metal sulfides and phosphides have attracted great attention in the hydrogen evolution reaction.[8] In other studies, an electrocatalyst consisting of iron phosphide (FeP) and graphene sheets and an electrocatalyst synthesized from nickel phosphide (Ni_2P) nanoparticles and reduced graphene oxide (rGO) doped with nitrogen were developed.[7,9] Structural characterization showed that high catalytic activity was associated with synergistic effects, promising carbon conductivity, and the presence of electron-rich nitrogen atoms.[3,7,10]

Transition metal-based spinel-type materials have rapidly become have emerged as promising and highly efficient active materials for potential electrochemical applications due to their numerous advantages such as low prices, abundant resources, and environmental friendliness.[11–13] Among the wide range of compounds, spinels containing cobalt, nickel or molybdenum are of particular interest as high-performance oxygen evolution reaction (OER) catalysts.[14,15] One example of the use of bimetallic oxides for HER and OER is $NiCo_2O_4$. It is characterized by good activity towards the evolution of oxygen and hydrogen.[16] The presence of transition metal particles such as cobalt and nickel, due to their conductivity and electron configurations, provides a large number of active sites and excellent electrochemical performance in the oxygen evolution reaction.[12,17] However, other bimetallic oxides, which will also be characterized by good electrocatalytic activity, should also be searched. Recently, electrode materials of spinel-type compounds containing cobalt and manganese have been intensively studied as a very promising electrocatalyst.[18] This material in the form of $MnCo_2O_4$ is also used for high-performance supercapacitors,[19] lithium-ion batteries,[20] photocatalytic CO_2 reduction,[21] and gas sensors.[22] However, to improve the electrochemical performance of spinel structures, a favorable strategy is the introduction of heteroatoms and integration with conducting materials.[18] In order to design a novel and highly active

[a]Faculty of Chemistry, Nicolaus Copernicus University in Torun, Gagarina 7, 87-100 Torun, Poland. E-mail: ailnicka@umk.pl

[b]Faculty of Chemistry, Department of Chemistry and Technology of Functional Materials, Gdańsk University of Technology, Narutowicza 11/12, 80-233 Gdańsk, Poland

[c]Advanced Materials Center, Gdańsk University of Technology, Narutowicza 11/12, 80-233 Gdańsk, Poland

[d]Centre for Modern Interdisciplinary Technologies, Nicolaus Copernicus University in Torun, Wilenska 4, 87-100 Torun, Poland

$MnCo_2O_4$/carbon based catalyst, various approaches have been investigated.[23,24] Only, the synergetic effect of the hybrid nanostructure may have a significant impact on the properties. In one of the strategies, the coupling of $MnCo_2O_4$ with carbon nanotubes (CNTs) and nitrogen-doped reduced graphene oxide (N-rGO) has been described. The OER performance of the $MnCo_2O_4$/N-rGO hybrid is comparable to the benchmark iridium-carbon catalyst due to enhanced conductivity and facilitated charge transfer.[18,25] Another approach proposed the introduction of heteroatoms such as nickel and zinc, followed by their combination with reduced graphene oxide ($Mn_{0.4}$-$Ni_{0.6}Co_2O_4$/rGO and $Mn_{0.8}Zn_{0.2}Co_2O_4$/rGO) is also an effective alternative.[26] The hybrid's high performance is mainly attributed to its unique morphology, more exposed active sites, and porous structure with a high specific surface area.[11,27]

The aim of the conducted research was to examine the influence of the ratios of reagents $MnCo_2O_4$/exfoliated graphite (EG) in hybrid structures for their catalytic properties. This work aimed to establish effective hybrid composition combining oxides of manganese and cobalt with electrochemically exfoliated cheap, commercially available graphite. The physicochemical properties of the obtained materials were characterized using different analytical techniques, such as high-resolution transmission electron microscopy (HRTEM), X-ray diffraction (XRD), Raman spectroscopy, and X-ray photoelectron spectroscopy (XPS). The electrochemical properties of hybrid nanostructures were tested in oxygen and hydrogen evolution reactions. It is very important to understand how the ratio of the reagents influences the properties of the final products obtained in the simple synthesis method and the possibility of their use for green hydrogen production.

The morphology of the obtained materials was determined by high-resolution transmission electron microscopy analysis. Fig. 1 on the left side shows the HRTEM images of the synthesized $MnCo_2O_4$ which have a crystal structure with particle size in the range of 10–30 nm, and the particles tend to agglomerate. Fig. 1 on the right side shows image of the obtained $MnCo_2O_4$/EG (2/1) hybrid nanostructure which consist of distinct $MnCo_2O_4$ structures uniformly dispersed on the graphene layer as indicated by the arrows. The hybrid nanostructure exhibit a lower tendency to agglomerate, compared to pure $MnCo_2O_4$. The HRTEM images for $MnCo_2O_4$/EG (1/1) and $MnCo_2O_4$/EG (1/2) in Fig. S1† reveal also that nanostructured $MnCo_2O_4$ with size with a broad range from 5 to 100 nm among carbon phase them have been successfully synthesised and dispersed in the carbon phase. Additionally, for samples $MnCo_2O_4$/EG (1/1) and
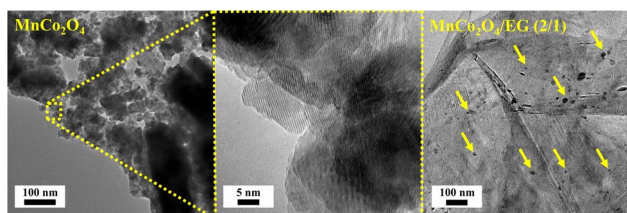
$MnCo_2O_4$/EG (1/2) agglomerated particles of $MnCo_2O_4$ with size more than 200 nm were identified.

X-ray diffraction patterns in Fig. 2(a) confirmed that synthesized $MnCo_2O_4$ is crystalline with a cubic spinel structure. The Bragg peaks at (111), (220), (311), (400), (422), (511), and (440) were assigned to $MnCo_2O_4$.[28] The intensity of peaks assigned to $MnCo_2O_4$ decrease with the increasing amount of carbon nanostructure in hybrid materials. An additional prominent peak was determined for $MnCo_2O_4$/EG hybrid structures located at about the angular value of 26.5°, which could indicate the existence of carbon. For two samples $MnCo_2O_4$/EG (2/1) and $MnCo_2O_4$/EG (3/1) with the highest amount of catalyst in the carbon phase additional peaks with low intensity were observed. The presence in these samples of small amount of Co_3O_4 contributed to these additional peaks may have been formed under the conditions of the synthesis procedure.

Raman spectroscopy was used to confirm the presence of carbon in the hybrid nanostructures as well as to check the composition of the prepared samples. Raman spectra for hybrid structures and pure $MnCo_2O_4$ and exfoliated graphite are present in Fig. 2(b). In all of the hybrid samples with exfoliated
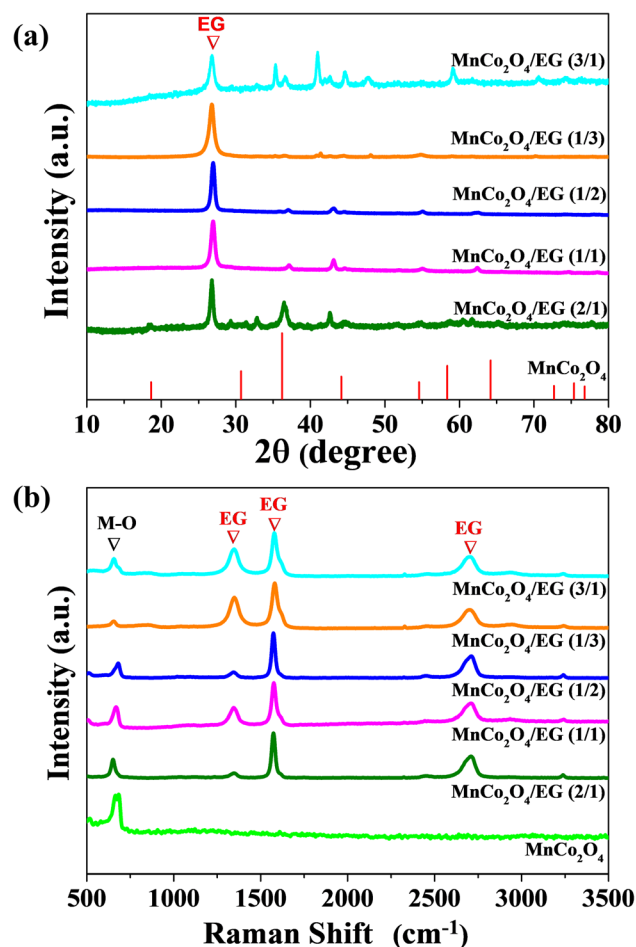

Fig. 1 HRTEM images of $MnCo_2O_4$ and $MnCo_2O_4$/EG (2/1).

Fig. 2 (a) X-ray diffraction patterns and (b) Raman spectra of $MnCo_2O_4$ and $MnCo_2O_4$/EG series.

graphite three prominent peaks at 1347 cm^{-1}, 1580 cm^{-1}, and 2708 cm^{-1} correspond to the D band, G band, and 2D band of carbon, respectively.[29] Analysis of intensity ratio of the D band to G band (I_D/I_G) is used to evaluate the disorder of carbon networks.[30,31] Intensity ratio of I_D/I_G for samples with exfoliated graphite is at the same low level for all samples in the range from 0.30 to 0.41 which indicate that EG do not possess many defected places. For pure MnCo$_2$O$_4$ particles, only one characteristic peak at 680 cm^{-1} corresponding to the stretching vibration mode of M–O (M = Mn, Co) was determined.[32,33] Also, in hybrid samples the peak for M–O is visible. However, the sample is not entirely homogeneous and in some places, a lack of response from M–O vibrations can be observed (see Fig. S2†).

X-ray photoelectron survey spectrum and high-resolution spectra are presented in Fig. 3 for the hybrid sample MnCo$_2$O$_4$/EG (2/1). Deconvolution of C1s spectra showed the most intense peaks are related to the carbon bonding attributed to C=C (284.4 eV) and C–C (284.9 eV).[34] Moreover, other functionalities, such as C–O–C, C–OH (286.3 eV), C=O, O–C–O (287.6 eV), O–C=O (288.5 eV), and π–π (290.1 eV and 292.7 eV)[35] formed on the surface of MnCo$_2$O$_4$/EG (2/1) hybrid sample. The formation of functional groups is confirmed by O1s XPS deconvolution obtained for MnCo$_2$O$_4$/EG (2/1), which reveals the presence of O–Me (529.8 eV), O–Me, O=C (531.6 eV), and O–C–O (532.6 eV). XPS deconvolution of the Co2p$_{3/2}$ spectrum was fitted with six lines, the first of which lying at a binding energy of 780.1 eV indicates the presence of Co^{3+},[36] while the line at 781.6 eV is assigned to Co^{2+}.[19] Deconvolution of the Mn2p$_{3/2}$ spectrum was fitted with five lines, two lines of which lying at a binding energy of 641.4 eV and 643.9 eV indicating the presence of Mn^{2+} (ref. 21) and Mn^{3+} (ref. 37) oxidation sites.

Hybrid materials of spinel oxide with carbon can be an excellent catalyst for water splitting efficiency, due to the potential application of obtained catalysts for hydrogen evolution reaction and oxygen evolution reaction. The linear sweep voltammetry of pure MnCo$_2$O$_4$ and obtained hybrid nanostructures was performed using the three-electrode system. The LSV curves at a scan rate of 1 mV s^{-1} in 1 M KOH for OER and

HER were performed. From the LSV curves for OER presented in Fig. 4(a), the OER activity was compared using the required overpotentials to achieve a current density of 10 mA cm^{-2} (η_{10}). For the obtained hybrid samples MnCo$_2$O$_4$/EG (2/1), MnCo$_2$O$_4$/EG (1/1), MnCo$_2$O$_4$/EG (1/2), MnCo$_2$O$_4$/EG (1/3), and MnCo$_2$O$_4$/EG (3/1) the overpotential was 1.66 V, 1.78 V, 1.75 V, 1.79 V, and 1.72 V, respectively. This overpotential was greatly improved for MnCo$_2$O$_4$/EG (2/1) compared with MnCo$_2$O$_4$ and even lower than the commercial RuO$_2$/IrO$_2$ catalyst (η_{10} = 1.71 V).
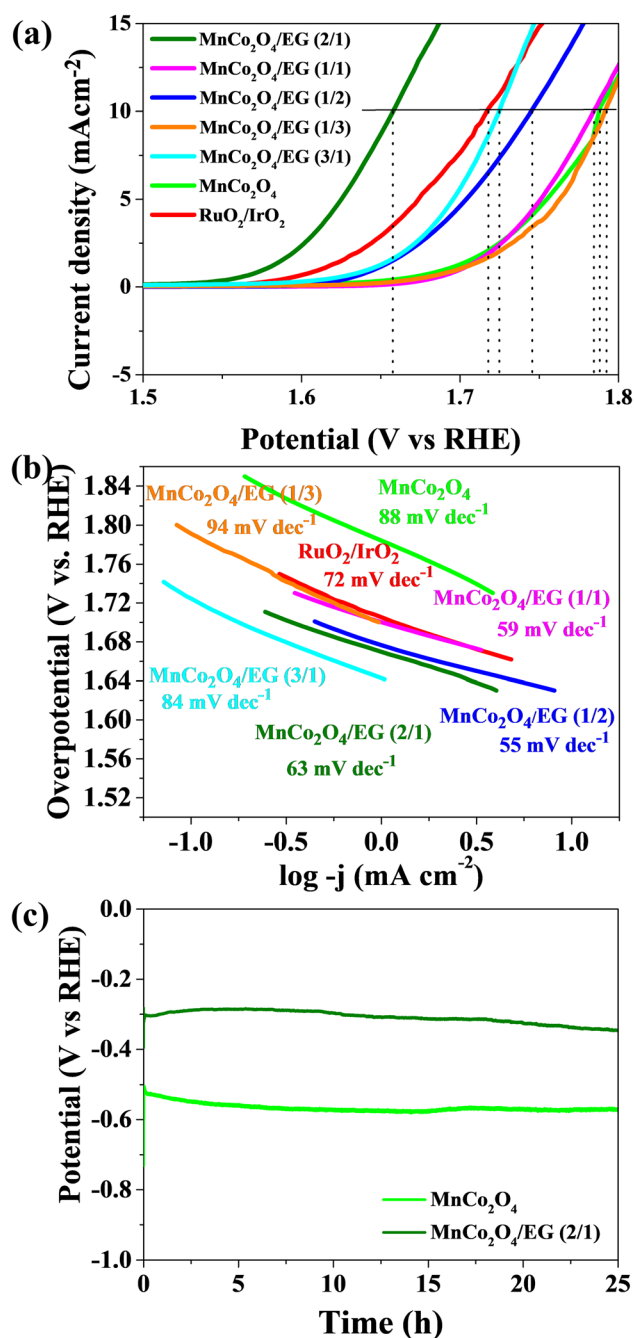

Fig. 4 (a) Linear seep voltammograms for the OER reaction in 1 M KOH. (b) Tafel plots determined from LSV in 1 M KOH. (c) Stability of MnCo$_2$O$_4$/EG (2/1) and RuO$_2$/IrO$_2$ at a current density of 10 mA cm^{-2}.
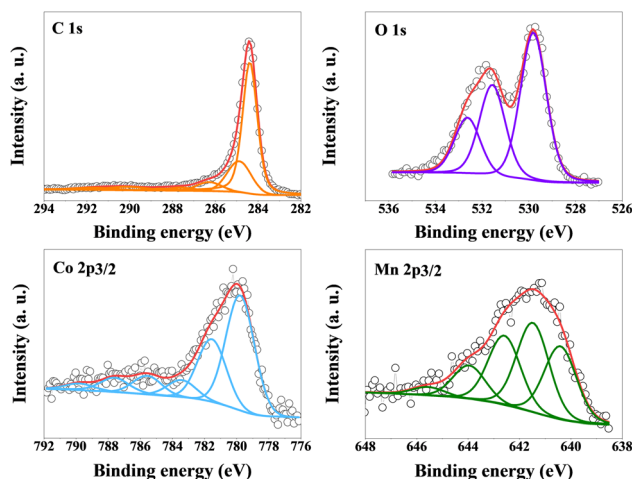

Fig. 3 High-resolution XPS spectra for MnCo$_2$O$_4$/EG (2/1) sample.

Therefore, the highest electrocatalytic activity approximate to commercial RuO$_2$/IrO$_2$ catalyst is shown by sample MnCo$_2$O$_4$/EG (2/1), for which the value of the potential obtained at the required current density is 1.66 V. This sample has the highest content of MnCo$_2$O$_4$ compare other hybrid catalysts. The OER kinetics were estimated using Tafel plots, and the linear region was fitted *via* the Tafel equation: $\eta = a + b \log j$, where η is the overpotential, j is the current density, and b is the Tafel slope. From Fig. 4(b), the calculated Tafel slope for hybrid catalysts is in the range 55–94 mV dec^{-1}, which is superior to that of commercial RuO$_2$/IrO$_2$ (72 mV dec^{-1}) and MnCo$_2$O$_4$ (83 mV dec^{-1}). As shown in Fig. 4(c), the addition of exfoliated graphite causes to the high electrochemical stability for sample MnCo$_2$O$_4$/EG (2/1) comparable to commercial RuO$_2$/IrO$_2$.

Besides the OER activity, excellent HER activity is also crucial for bifunctional catalysts. The results of measurements of HER obtained by the linear sweep voltammetry in 1 M KOH for the tested materials are shown in Fig. 5(a). The results for glassy carbon electrode (GCE) have been included in the manuscript for comparison purposes. As can be seen, GCE shows no activity compared to the other catalysts. To evaluate the performance of the obtained catalysts, the potential obtained at a current density of −10 mA cm^{-2} was compared for this electrolyte, and all of the tested samples achieved the required current density. The apparent improvement in the overpotential for the hybrids is evidence that the materials, when combined with exfoliated graphite, show improved performance in HER in 1 M KOH electrolyte than pure MnCo$_2$O$_4$. The polarization curves measured in basic electrolyte show a sharp decrease in the current density as the potential decrease and have an overpotential of −0.39 V, −0.49 V, −0.49 V, 0.58, and 0.49 for hybrid samples obtained in mass ratio 2/1, 1/1, 1/2, 1/3, and 3/1 (MnCo$_2$O$_4$ to EG), respectively.

Among of hybrid materials, sample MnCo$_2$O$_4$/EG (2/1) shows the best catalytic activity and achieved the required current density at a potential value of −0.39 V. Furthermore, this effect is because graphene sheets serve a conducting support, causing enhanced electrical conductivity. This ratio 2/1 of MnCo$_2$O$_4$ to EG, where we have lower amount of carbon allows for uniform dispersion of MnCo$_2$O$_4$ on the exfoliated graphite surface and obtaining form distribution of particles beneficial in the HER response. The high catalytic activity may have resulted from the high carbonization temperature, which increased the conductivity of the material. From Fig. 5(b), the calculated Tafel slope for hybrid catalysts are in the range of 109–374 mV dec^{-1}, which is still higher than for commercial Pt/C (88 mV dec^{-1}). When we compare these results of hybrids with MnCo$_2$O$_4$ (113 mV dec^{-1}) only sample MnCo$_2$O$_4$/EG (2/1) (109 mV dec^{-1}) is superior.

The electrochemical stability of materials is an important parameter which determines commercial application, stability test results are presented in Fig. 5(c). The stability of the hybrid catalyst MnCo$_2$O$_4$/EG (2/1) did not change significantly compared to commercial Pt/C after 24 h, meaning that this material is stable during electrochemical measurements.

The ECSA (electrochemically active surface area) was determined to elucidate the effect of composition on HER and OER. The ECSA was estimated using the CV method's double-layer
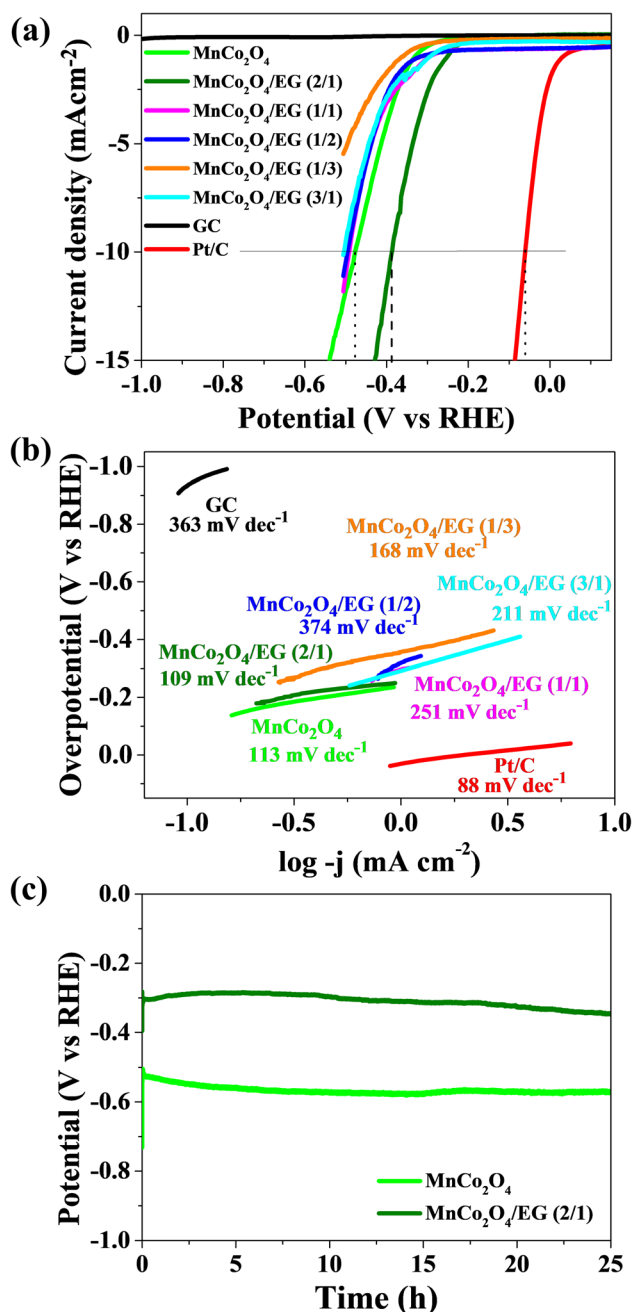

Fig. 5 (a) Linear seep voltammograms for the HER reaction in 1 M KOH. (b) Tafel plots determined from LSV in 1 M KOH. (c) Stability of MnCo$_2$O$_4$/EG (2/1) and Pt/C at a current density of −10 mA cm^{-2}.

capacitance in KOH electrolyte. Fig. S3† shows the CV for obtained catalysts performed in the non-faradaic region at different scanning rates. For the all obtained electrodes in two electrolytes, the charging current at the different scan rates was plotted (Fig. S4†) to obtain the double-layer capacitance from the slope. As can be seen, ECSA differs from the electrolyte used. The ECSA was estimated using the commonly used specific capacity of 0.04 mF cm^{-2}.[38] Results are summarized in Table S1.† Although the MnCo$_2$O$_4$/EG (1/3) catalyst has by far the highest ECSA, this does not affect the better catalytic properties.

In conclusion, in this case, the ECSA does not have much influence on the catalytic activity.

This work presents a facile production method of $MnCo_2O_4$/exfoliated graphite hybrid structures with desired electrochemical properties was proposed. The proposed preparation method leads to the efficient dispersion of $MnCo_2O_4$ crystallites between carbon sheets with a low tendency to agglomerate of the synthesized nanoparticles, which was confirmed by HRTEM analysis. The obtained spinel $MnCo_2O_4$ structures on exfoliated graphite were tested in HER and OER reactions. The results indicated that the addition of exfoliated graphite increases the catalytic activity of the $MnCo_2O_4$, as well as increases the sample's electron conductivity. The analyzed electrochemical properties in KOH electrolyte for OER have shown that $MnCo_2O_4$/EG obtained with a ratio of 2 : 1 enhanced better catalytic activity because overpotential was lower than for samples obtained with 1 : 1 and 1 : 2 ratio of $MnCo_2O_4$ to EG. The Tafel slope calculated from LSV measured in OER for hybrid catalysts was lower than for commercial RuO_2/IrO_2 and pure $MnCo_2O_4$. The analyzed electrochemical properties in the KOH electrolyte for HER have shown that the addition of carbon for $MnCo_2O_4$ causes to the increase of overpotential and besides $MnCo_2O_4$/EG (2/1) sample remaining analyzed hybrid catalysts possess similar values of overpotential. In summary, the presented new hybrid structures are bifunctional alkaline catalysts, exhibiting excellent electrocatalytic performance and very good working stability for both the HER and OER.

Conflicts of interest

There are no conflicts to declare.

Acknowledgements

Notes and references

1 S. Shit, S. Bolar, N. C. Murmu and T. Kuila, *J. Energy Chem.*, 2021, **59**, 160–190.

2 Y. Li, L. Zhou and S. Guo, *EnergyChem*, 2021, **3**, 100053.

3 X. Wang, A. Vasileff, Y. Jiao, Y. Zheng and S.-Z. Qiao, *Adv. Mater.*, 2019, **31**, 1803625.

4 J. Zhu, L. Hu, P. Zhao, L. Y. S. Lee and K.-Y. Wong, *Chem. Rev.*, 2019, **120**, 851–918.

5 X. Peng, C. Pi, X. Zhang, S. Li, K. Huo and P. K. Chu, *Sustainable Energy Fuels*, 2019, **3**, 366–381.

6 I. K. Sideri and N. Tagmatarchis, *Chem.–Eur. J.*, 2020, **26**, 15397–15415.

7 M. A. Younis, S. Lyu, Q. Zhao, C. Lei, P. Zhang, B. Yang, Z. Li, L. Lei, Y. Hou and X. Feng, *BMC Mater.*, 2019, **1**, 1–26.

8 C. Lu, D. Tranca, J. Zhang, F. n. Rodríguez Hernández, Y. Su, X. Zhuang, F. Zhang, G. Seifert and X. Feng, *ACS Nano*, 2017, **11**, 3933–3942.

9 S. S. Shinde, A. Sami and J. H. Lee, *ChemCatChem*, 2015, **7**, 3873–3880.

10 J. Cao, C. Lei, J. Yang, X. Cheng, Z. Li, B. Yang, X. Zhang, L. Lei, Y. Hou and K. K. Ostrikov, *J. Mater. Chem. A*, 2018, **6**, 18877–18883.

11 P. V. Shinde, R. Samal and C. S. Rout, *Trans. Tianjin Univ.*, 2022, **28**, 80–88.

12 A. Dymerska, W. Kukułka, M. Biegun and E. Mijowska, *Materials*, 2020, **13**, 3918.

13 L. Liu and Y. Xiao, *Comput. Mater. Sci.*, 2021, **187**, 110082.

14 Z. Li, M. Hu, P. Wang, J. Liu, J. Yao and C. Li, *Coord. Chem. Rev.*, 2021, **439**, 213953.

15 J. Zhou, J. Li, L. Zhang, S. Song, Y. Wang, X. Lin, S. Gu, X. Wu, T.-C. Weng and J. Wang, *J. Phys. Chem. C*, 2018, **122**, 14447–14458.

16 X. Gao, H. Zhang, Q. Li, X. Yu, Z. Hong, X. Zhang, C. Liang and Z. Lin, *Angew. Chem., Int. Ed.*, 2016, **55**, 6290–6294.

17 Y. Xu, K. Fan, H. Q. Fu, Y. Zou, M. Dong, Y. Dou, Y. Wang, S. Chen, H. Yin and M. Al-Mamun, *Nanoscale*, 2021, **13**, 20324–20353.

18 K. Lankauf, K. Cysewska, J. Karczewski, A. Mielewczyk-Gryń, K. Górnicka, G. Cempura, M. Chen, P. Jasiński and S. Molin, *Int. J. Hydrogen Energy*, 2020, **45**, 14867–14879.

19 Y. Dong, Y. Wang, Y. Xu, C. Chen, Y. Wang, L. Jiao and H. Yuan, *Electrochim. Acta*, 2017, **225**, 39–46.

20 A. K. Mondal, D. Su, S. Chen, A. Ung, H. S. Kim and G. Wang, *Chem.–Eur. J.*, 2015, **21**, 1526–1532.

21 S. Wang, Y. Hou and X. Wang, *ACS Appl. Mater. Interfaces*, 2015, **7**, 4327–4335.

22 S. Vadivel, G. Balaji and S. Rathinavel, *Opt. Mater.*, 2018, **85**, 267–274.

23 C. Sun, J. Yang, Z. Dai, X. Wang, Y. Zhang, L. Li, P. Chen, W. Huang and X. Dong, *Nano Res.*, 2016, **9**, 1300–1309.

24 X. Ge, Y. Liu, F. T. Goh, T. A. Hor, Y. Zong, P. Xiao, Z. Zhang, S. H. Lim, B. Li and X. Wang, *ACS Appl. Mater. Interfaces*, 2014, **6**, 12684–12691.

25 X.-M. Liu, X. Cui, K. Dastafkan, H.-F. Wang, C. Tang, C. Zhao, A. Chen, C. He, M. Han and Q. Zhang, *J. Energy Chem.*, 2021, **53**, 290–302.

26 J. M. Gonçalves, M. N. T. Silva, K. K. Naik, P. R. Martins, D. P. Rocha, E. Nossol, R. A. A. Munoz, L. Angnes and C. S. Rout, *J. Mater. Chem. A*, 2021, **9**, 3095–3124.

27 J. Yu, J. Dai, Q. He, D. Zhao, Z. Shao and M. Ni, *Mater. Rep.: Energy*, 2021, **1**, 100024.

28 S. Jayasubramaniyan, S. Balasundari, P. Rayjada, R. A. Kumar, N. Satyanarayana and P. Muralidharan, *J. Mater. Sci.: Mater. Electron.*, 2018, **29**, 21194–21204.

29 D. Yang, A. Velamakanni, G. Bozoklu, S. Park, M. Stoller, R. D. Piner, S. Stankovich, I. Jung, D. A. Field and C. A. Ventrice Jr, *Carbon*, 2009, **47**, 145–152.

30 A. Guedes, B. Valentim, A. C. Prieto, S. Rodrigues and F. Noronha, *Int. J. Coal Geol.*, 2010, **83**, 415–422.

31 F. C. Tai, S. C. Lee, J. Chen, C. Wei and S. H. Chang, *J. Raman Spectrosc.*, 2009, **40**, 1055–1059.

32 L.-C. Chen, Z. Chen, Y.-H. Huang, H.-S. Hou, *nternational Conference on Advanced Materials for Science and Engineering (ICAMSE)*, 2016, pp. 653–656.

33 J. Baraliya, *AIP Conf. Proc.*, 2016, 060020.

34 C. Moreno-Castilla, M. López-Ramón and F. Carrasco-Marın, *Carbon*, 2000, **38**, 1995–2001.

35 J. D. Ding, Y. F. Diao and H. G. Shen, *Adv. Mater. Res.*, 2011, 1211–1214.

36 R. Huang, J. Lin, J. Zhou, E. Fan, X. Zhang, R. Chen, F. Wu and L. Li, *Small*, 2021, **17**, 2007597.

37 S. G. Krishnan, M. Harilal, N. Arshid, P. Jagadish, M. Khalid and L. P. Li, *J. Energy Storage*, 2021, **44**, 103566.

38 P. Connor, J. Schuch, B. Kaiser and W. Jaegermann, *Z. Phys. Chem.e*, 2020, **234**, 979–994.